Elsevier Editorial System(tm) for Advances in Space Research
Manuscript Draft

Manuscript Number:

Title: Validation of plasmasphere electron density reconstructions derived from data on board CHAMP by IMAGE/RPI data

Article Type: EM

Keywords: Plasmasphere, Ionosphere, IMAGE, CHAMP, Electron Density, Total Electron Content

Corresponding Author: Dr. Tatjana Gerzen, PhD

Corresponding Author's Institution: German Aerospace Center (DLR)

First Author: Tatjana Gerzen, PhD

Order of Authors: Tatjana Gerzen, PhD; Joachim Feltens, Dr. ; Norbert Jakowski, Dr. ; Ivan Galkin; Richard Denton; Bodo Reinisch

Abstract: Plasmaspheric electron content is, beyond the ionosphere as major source, a significant contributor to the overall TEC budget affecting GNSS signals. The plasmasphere can induce half or more of the GNSS range errors caused by atmospheric electrical charges, in particular at nighttime. At DLR Neustrelitz, Germany, GPS measurements recorded onboard the LEO satellite CHAMP were used to reconstruct the topside electron density distribution (ionosphere & plasmasphere) up to GPS altitude, applying a model-based assimilation technique. In this paper, the potential of these CHAMP topside reconstructions for analyzing space weather related changes in the geo-plasma is investigated. For this purpose, comparisons are made between the CHAMP reconstructed profiles and electron densities derived from passive radio wave observations by the IMAGE RPI instrument for years 2001 till 2005.
The comparison results indicate that an improvement, compared to the electron density of a background model, can be achieved by CHAMP data assimilation. The improvement is especially visible in the L-shell region below 3, which contributes notably to the GNSS signal delays. However, for the region around the plasmapause, systematical electron density underestimations of the background model w.r.t. the IMAGE data are detected. The rather limited CHAMP data coverage and the degraded observation geometry at these high altitudes seem to be not sufficient for complete compensation of this underestimation during the assimilation procedure.
The results presented in this paper demonstrate the strengths of LEO TEC data assimilation, but at the same time illustrate the necessity to improve the modelling of the plasmasphere region above 4 ER L-shell distances. Furthermore, they reveal the need of additional data to establish an appropriate data base for the modelling of the complete plasmasphere.

Suggested Reviewers: Peter Chi
pchi@igpp.ucla.edu

Stefan Schlueter
stefan.schlueter@esa.int

Anna Belehaki

abeleha@OTENET.GR

Doug Menietti
jdm@space.physics.uiowa.edu

Figure

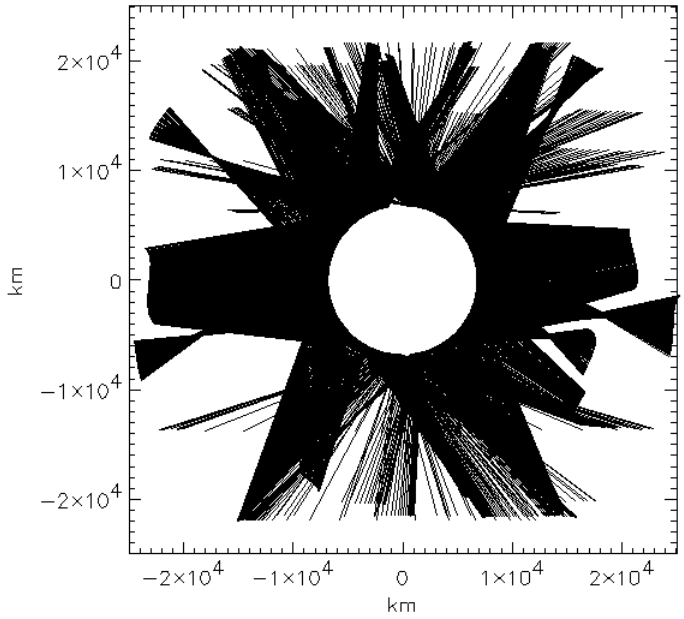

Fig. 1: The topside radio link distribution, projected into the plane of the mean CHAMP longitude, to the visible GPS satellites during one CHAMP revolution; 09.08.2001, 3331 TEC measurements (from Heise, 2003).

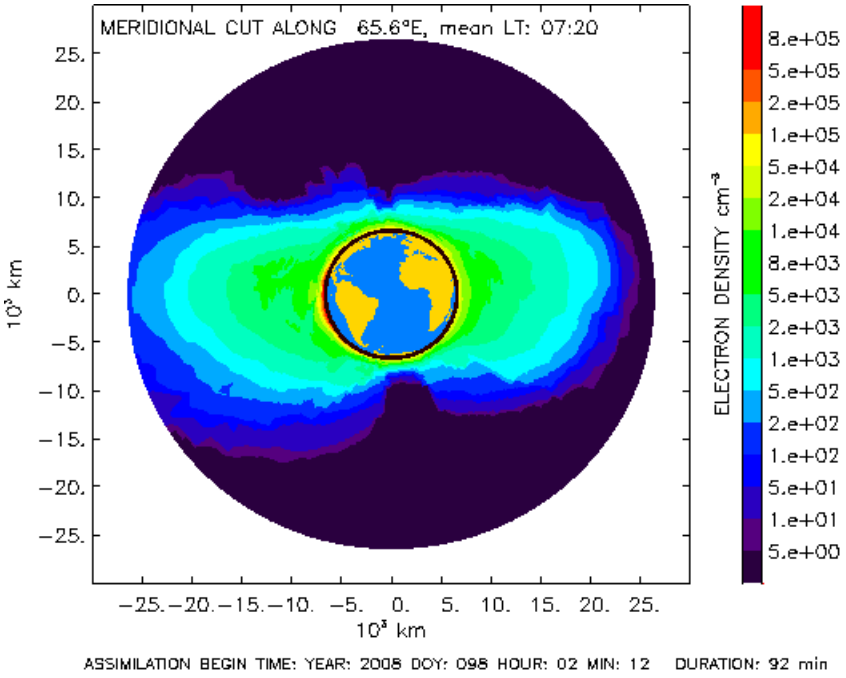

Fig. 2: Example of a CHAMP reconstruction showing an one CHAMP orbit revolution picture of the ionospheric and plasmaspheric electron density in the plane of the mean CHAMP orbit longitude.

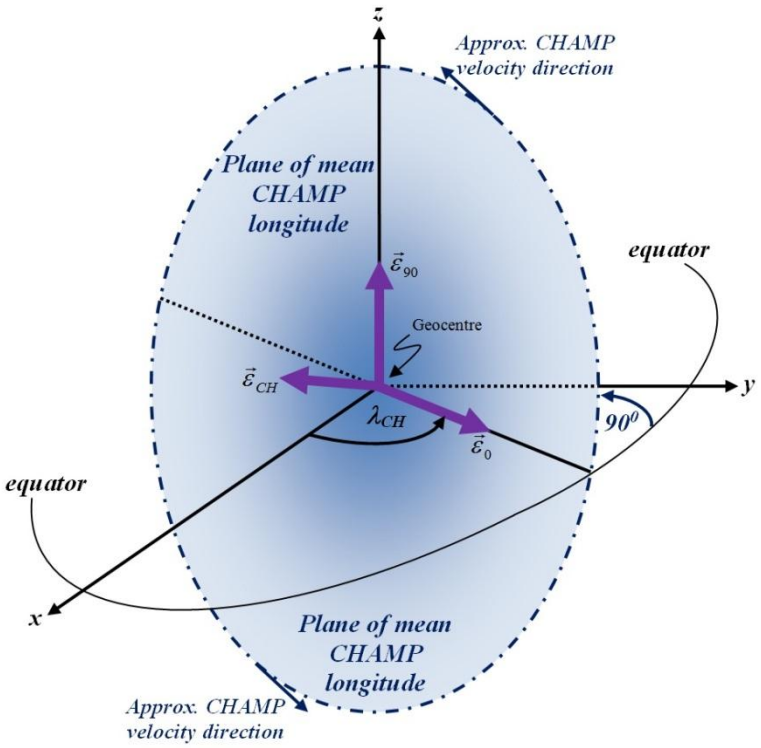

Fig. 3: The unit vectors defining the plane of mean CHAMP longitude (indicated as blue "disk") coordinate system.

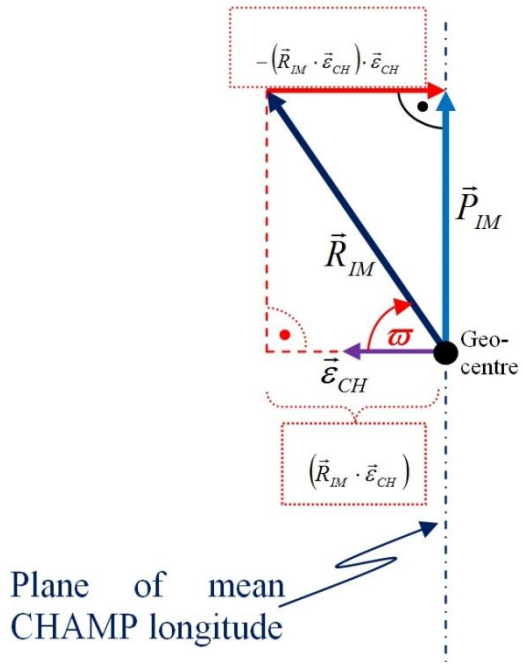

Fig. 4: The orthogonal projection $\vec{P}_{IM}$ of the IMAGE observation point position vector $\vec{R}_{IM}$ onto the CHAMP 2D reconstruction plane (displayed here edge-on as dash-dotted line).

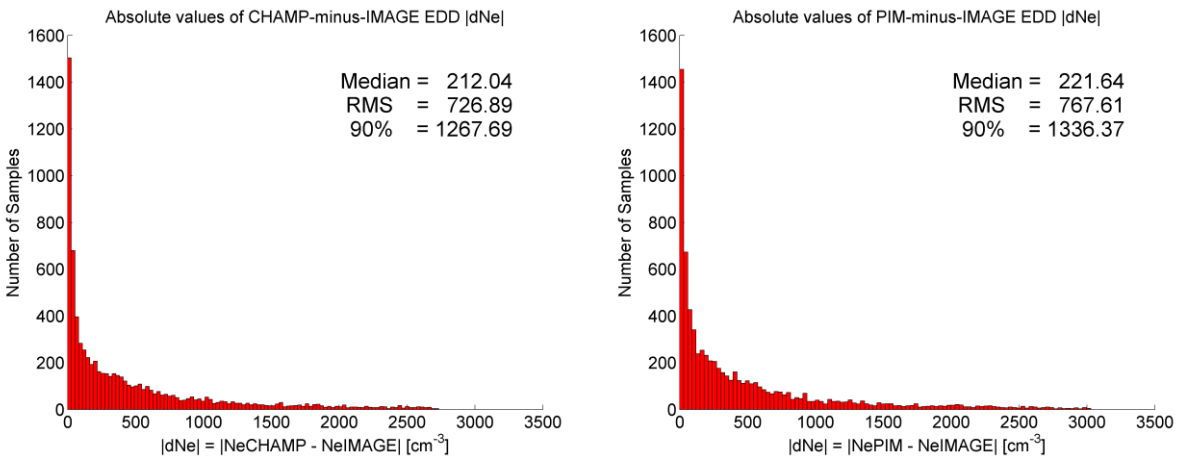

Fig. 5: Distribution of the absolute values of the CHAMP-IMAGE (left), PIM-IMAGE (right) EDD. Additionally the Median, RMS and 90% bound values of the absolute values of the EDD are given in the upper right corners. All values in cm^{-3}.

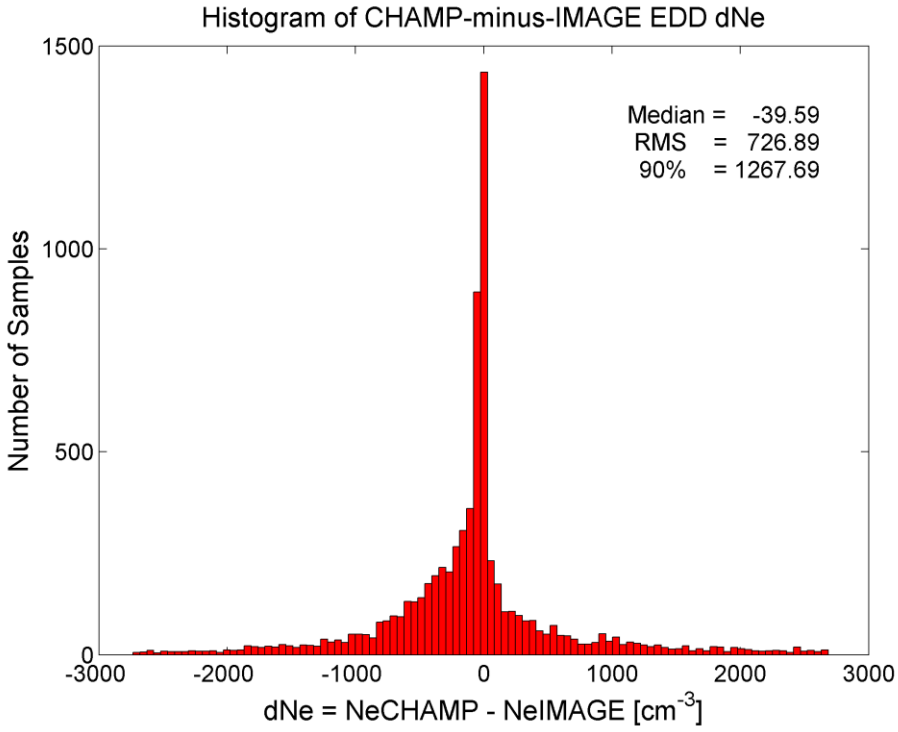

Fig. 6: Distribution of the CHAMP-IMAGE EDD. Additionally the Median, RMS and 90% bound values are given in the upper right corner. All values in cm^{-3}.

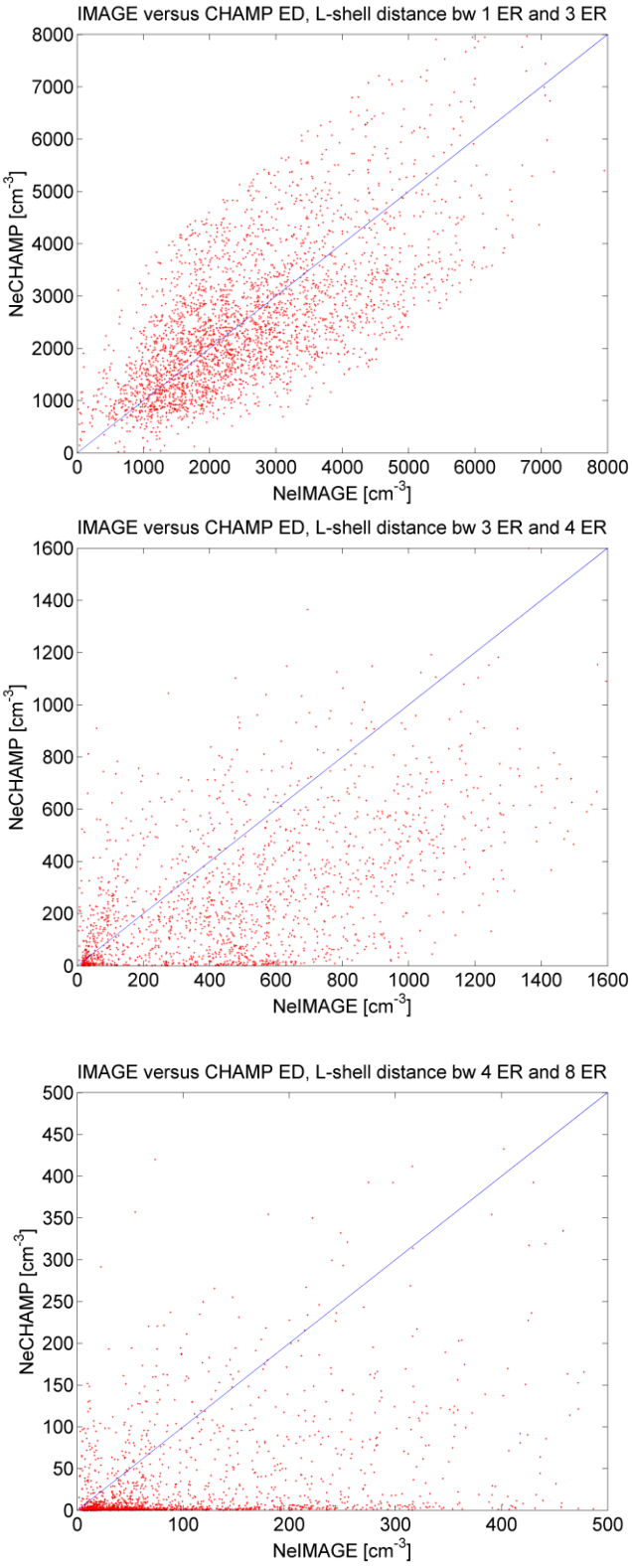

Fig. 7: Scatterplots of IMAGE versus CHAMP ED for *L*-shell distances (from top to bottom): between 1 ER and 3 ER, between 3 ER and 4 ER, between 4 ER and 8 ER.

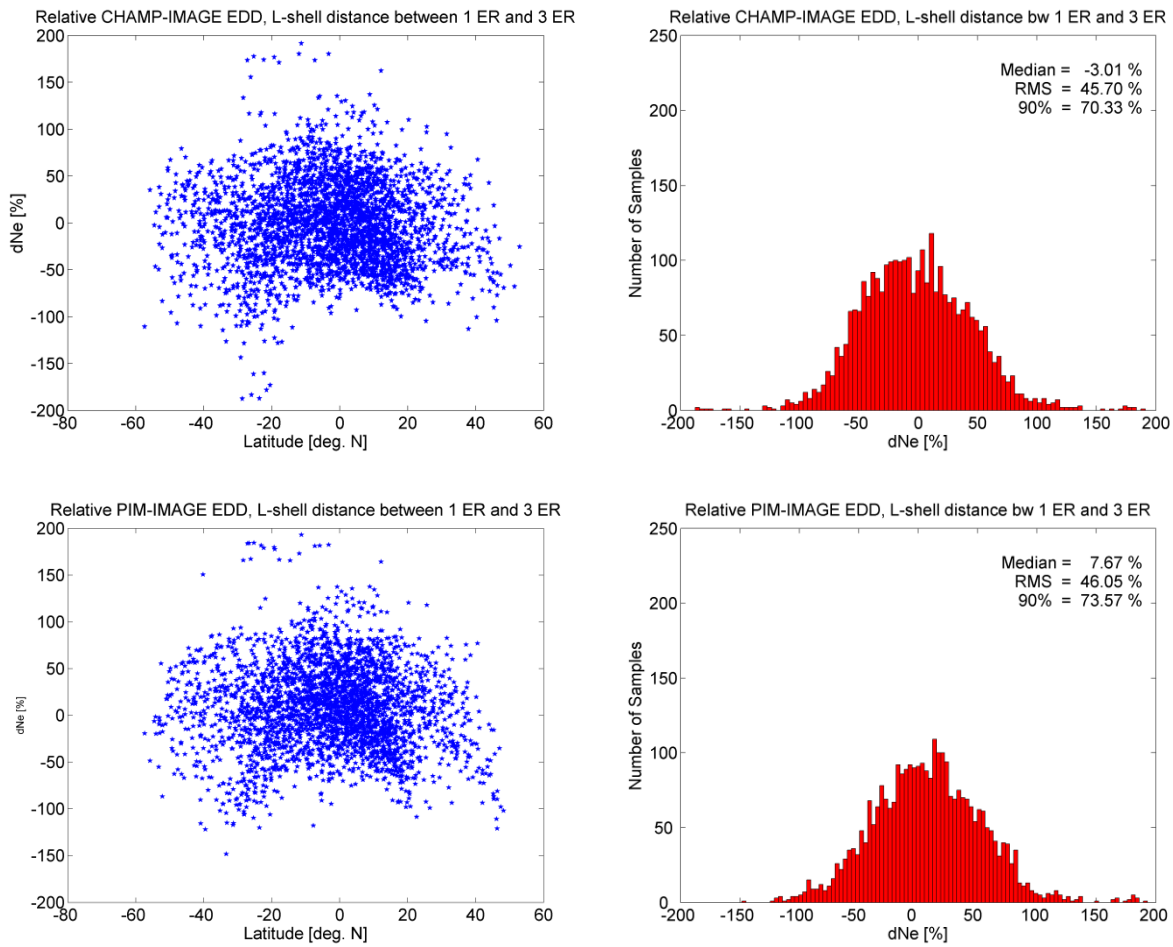

Fig. 8: Left hand side: Relative CHAMP-IMAGE EDD (top) and PIM-IMAGE EDD (bottom) versus geographic latitude. Right hand side: Distribution of the relative CHAMP-IMAGE EDD (top) and PIM-IMAGE EDD (bottom) for *L*-shell distances between 1 ER and 3 ER.

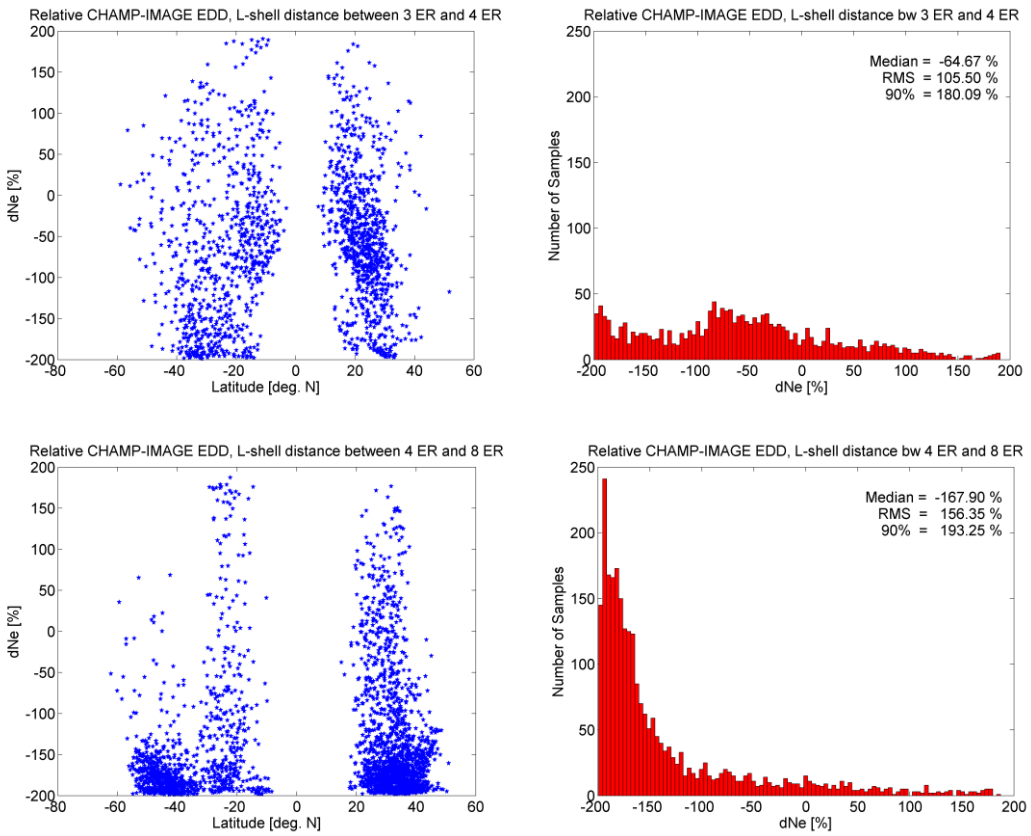

Fig. 9: Relative CHAMP-IMAGE EDD versus geographic latitude (left) and distribution of the relative CHAMP-IMAGE EDD (right) for *L*-shell distances (from top to bottom): between 3 ER and 4 ER, between 4 ER and 8 ER.

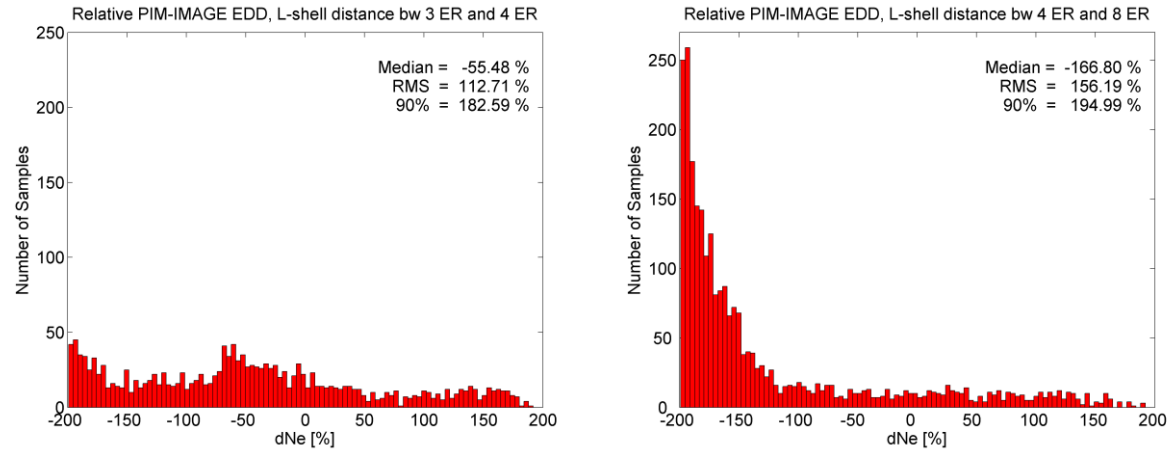

Fig. 10: Distribution of the relative PIM-IMAGE EDD for *L*-shell distances: between 3 ER and 4 ER (left), between 4 ER and 8 ER (right).

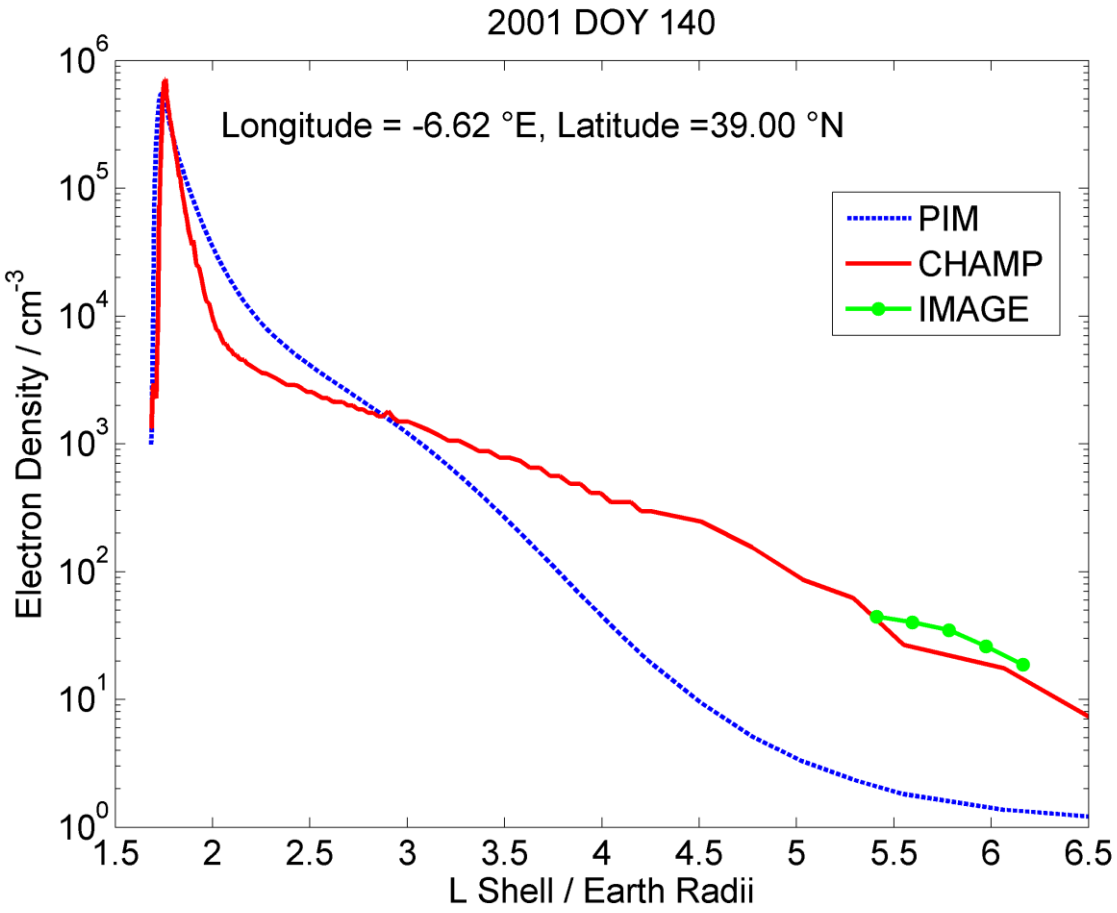

Fig. 11: Electron density profiles for DOY 140 of 2001 at geographic latitude of 39 °N and longitude of -6.62 °E. Reconstructed CHAMP profile in red, PIM calculated profile in blue dashed, IMAGE in green, here the observations are marked by dots.

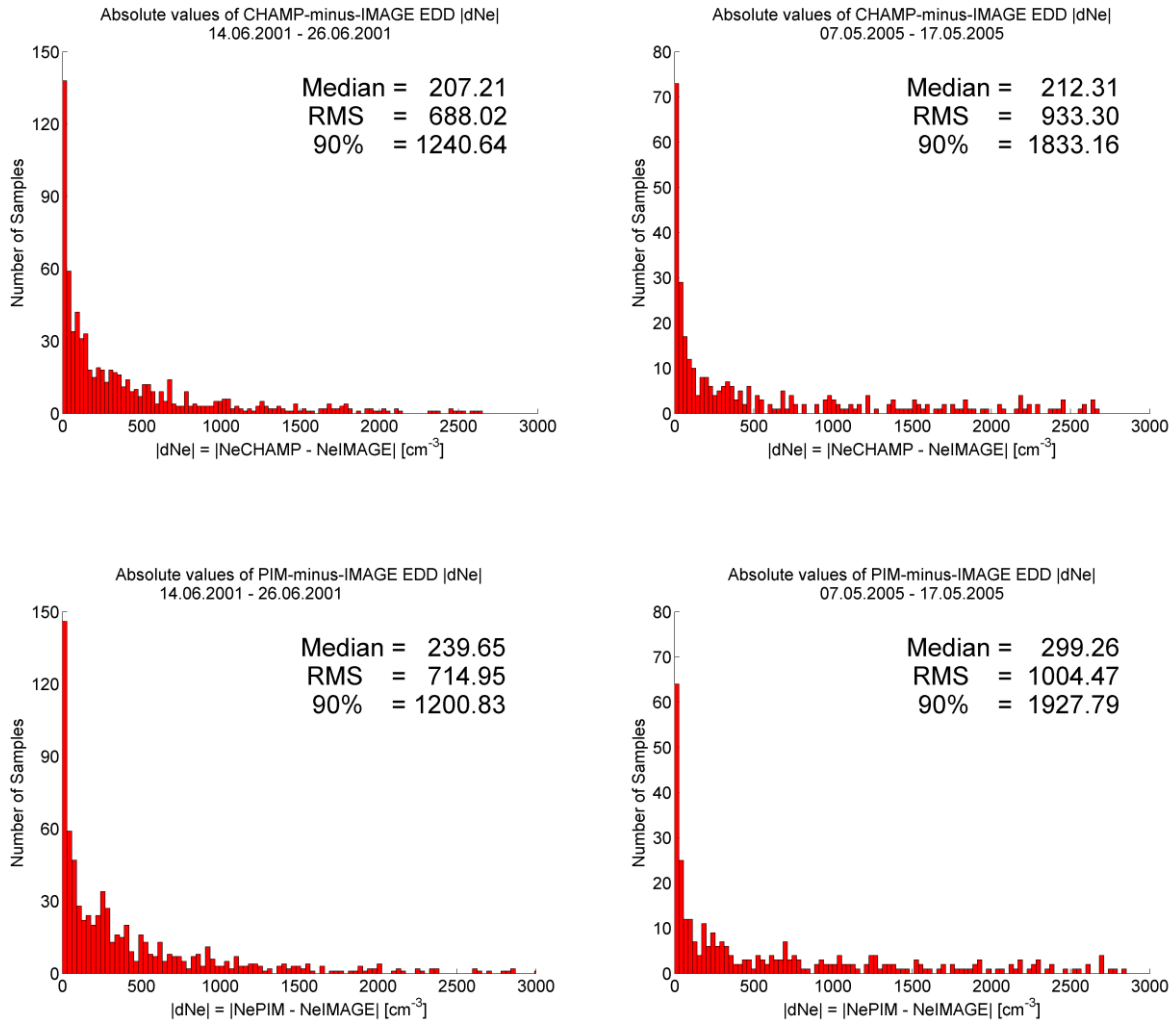

Fig. 12: Distribution of the absolute-values of the CHAMP-IMAGE (top), PIM-IMAGE (bottom) EDD. Left column: During the first time period (14.06.2001-26.06.2001). Right column: During the second time period (07.05.2005-17.05.2005). Additionally the Median, RMS and 90% bound values of the absolute-values of the EDD are given in the upper right corners. All values in cm^{-3}.

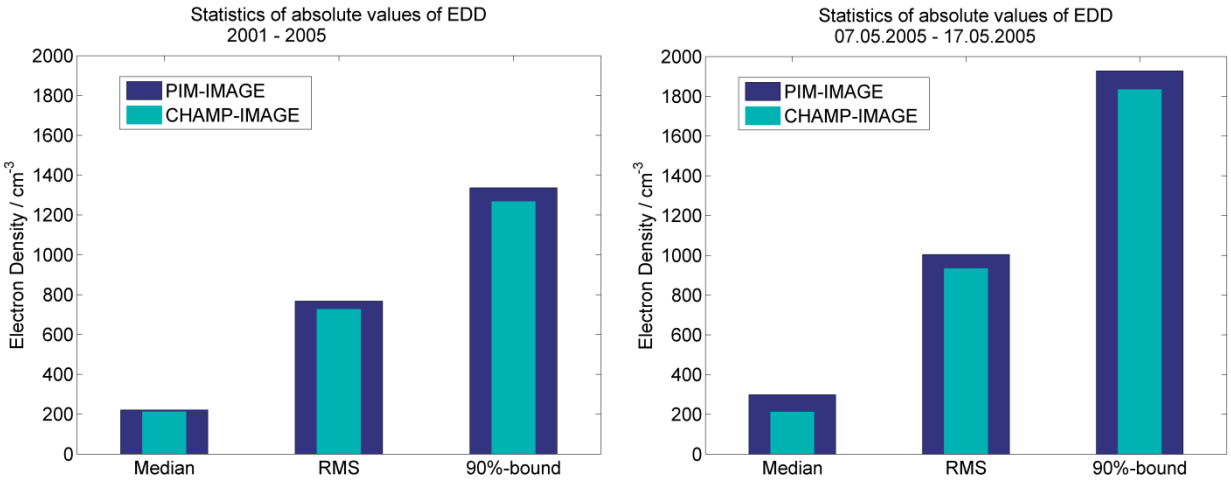

Fig. 13: Median, RMS and 90% bound values of the absolute values of the EDD. PIM values are presented in dark-blue, CHAMP values in pale blue. Left hand side: whole investigated time period (2001-2005). Right hand side: second disturbed time period (07.05.2005-17.05.2005).

Validation of plasmasphere electron density reconstructions derived from data on board CHAMP by IMAGE/RPI data

T. Gerzen[1], J. Feltens[2], N. Jakowski[1], I. Galkin[3], R. Denton[4], B. Reinisch[3], R. Zandbergen[5]

[1] *German Aerospace Center (DLR), Institute of Communications und Navigation (IKN), Kalkhorstweg 53, D-17235 Neustrelitz, Germany, phone:0049 (0) 3981 480 198, fax: 0049 (0) 3981 480 123, Tatjana.Gerzen@dlr.de*

[2] *Telespazio VEGA Deutschland GmbH c/o European Space Operations Centre (ESA/ESOC), Robert-Bosch-Straße 5, D-64293 Darmstadt, Germany, Joachim.Feltens@telespazio-vega.de*

[3] *Center for Atmospheric Research, University of Massachusetts Lowell, Lowell, Massachusetts, USA, Ivan_Galkin@uml.edu and Bodo.Reinisch@Digisonde.com*

[4] *Department of Physics and Astronomy, Dartmouth College, Hanover, New Hampshire, USA, redenton@gmail.com*

[5] *European Space Operations Centre (ESA/ESOC), Robert-Bosch-Straße 5, D-64293 Darmstadt, Germany, Rene.Zandbergen@esa.int*

Abstract
Plasmaspheric electron content is, beyond the ionosphere as major source, a significant contributor to the overall TEC budget affecting GNSS signals. The plasmasphere can induce half or more of the GNSS range errors caused by atmospheric electrical charges, in particular at nighttime. At DLR Neustrelitz, Germany, GPS measurements recorded onboard the LEO satellite CHAMP were used to reconstruct the topside electron density distribution (ionosphere & plasmasphere) up to GPS altitude, applying a model-based assimilation technique. In this paper, the potential of these CHAMP topside reconstructions for analyzing space weather related changes in the geo-plasma is investigated. For this purpose, comparisons are made between the CHAMP reconstructed profiles and electron densities derived from passive radio wave observations by the IMAGE RPI instrument for years 2001 till 2005.

The comparison results indicate that an improvement, compared to the electron density of a background model, can be achieved by CHAMP data assimilation. The improvement is especially visible in the *L*-shell region below 3, which contributes notably to the GNSS signal delays. However, for the region around the plasmapause, systematical electron density underestimations of the background model w.r.t. the IMAGE data are detected. The rather limited CHAMP data coverage and the degraded observation geometry at these high altitudes seem to be not sufficient for complete compensation of this underestimation during the assimilation procedure.

The results presented in this paper demonstrate the strengths of LEO TEC data assimilation, but at the same time illustrate the necessity to improve the modelling of the plasmasphere region above 4 ER *L*-shell distances. Furthermore, they reveal the need of additional data to establish an appropriate data base for the modelling of the complete plasmasphere.

Keywords: Plasmasphere, Ionosphere, IMAGE, CHAMP, Electron Density, Total Electron Content

1. Introduction

The plasmasphere is the upper part of the ionized and co-rotating atmosphere extending up to the plasmapause height which describes the boundary to the outer magnetosphere. The transition height, where ionospheric oxygen ion and proton densities balance, is located at about 1000 km altitude (e.g. Titheridge, 1976). In early beacon satellite studies, simultaneous Faraday rotation

and differential Doppler measurements were used to determine the plasmasphere electron content from about 2000-3000 km upwards (e.g. Poletti-Liuzzi et al., 1976). Such beacon studies revealed a plasmasphere electron content in the order of about 3-5 TECU. The plasmasphere electron content measured from about 1000 km upward should be somewhat bigger, in agreement with estimations by Belehaki et al. (2003), based on a comparison of GPS derived vertical total electron content (VTEC) and ionospheric TEC (ITEC) up to about 1000km height, estimated from vertical sounding data over Athens, Greece.

The plasma in the plasmasphere is closely coupled to the ionospheric plasma below 1000 km altitude. So the plasmasphere is filled up during daytime and acts as a plasma reservoir to maintain the ionospheric ionization at nighttime (Lunt et al., 1999). Strong plasma fluxes may even cause nighttime enhancements of plasma density in the ionosphere (Jakowski et al., 1991) or abnormally high ionization levels at winter nights (Jakowski et al. 1995). During geomagnetic storms, the plasmasphere is eroded due to the electric fields of magnetospheric origin. The refilling process typically requires several days during the recovery phase of the storm (Belehaki et al, 2003; Jakowski et al., 2007) although shorter refilling times of only one day have been reported (Reinisch et al., 2004).

The installation of dual frequency GPS receivers on board of LEO (Low Earth Orbiting) satellites, such as CHAMP (cf. Reigber et al., 2000), offers additional opportunity of ionospheric sounding, especially in the topside ionosphere and plasmasphere. To retrieve the topside electron density distribution from space-based observations, Heise et al. (2002) have developed a reconstruction technique that assimilates the GPS measurements onboard CHAMP into the Parameterized Ionospheric Model (PIM) (Daniell et al., 1995). This algorithm is used at DLR to generate electron density reconstructions of the topside ionosphere and plasmasphere.

To improve the use of the CHAMP topside reconstructions for analyzing space weather related changes in the geo-plasma, the accuracy of these data is checked in the present paper by comparing the reconstruction results with in situ electron density measurements onboard the IMAGE satellite (Reinisch et al., 2001). In Heise et al. (2002) first validation checks of the reconstruction results were performed at the CHAMP orbit height by comparison with the in situ plasma density measurements of the Planar Langmuir Probe on board CHAMP. The validation presented in this paper evaluates the reconstruction results and also the PIM modelled results at altitudes up to 20.000 km height.

Heise (2003) derived the RMS value of the estimated instrumental biases, calculated within the assimilation procedure to calibrate the CHAMP GPS measurements, to be around 0.5 TECU. The ionospheric region with geocentric distances above 3 Earth Radii (ER) contributes to the total electron content usually with less than 1 TECU. This means that TEC within this region is on the same accuracy level as the CHAMP GPS observations used for the assimilation. Furthermore, considering the CHAMP GPS measurement geometry, Heise et al. (2002) noticed the missing CHAMP GPS data coverage in the polar regions caused by the 55° inclination of the GPS orbit planes. Significant improvement by CHAMP GPS data assimilation can therefore be anticipated only in the region with L-shell distances below ~3 ER. In the present paper we assessed the accuracy of the reconstruction results separately for $1<L<3$, $3<L<4$, and $4<L<8$. Although no significant improvements were expected for $L>4$, the analysis for this outer part of the plasmasphere yielded instructive results, especially with regard to the overall statistics and the impact of the background model.

The paper is set up as follows: Details of the IMAGE Radio Plasma Imager (RPI) data and the CHAMP reconstructed electron density profiles are described in Sec. 2. Sec. 3 explains the data comparison technique itself, discussing the coincidence criteria and an approach for the coincidence analysis. Sec. 4 presents the results of the CHAMP-IMAGE and PIM-IMAGE comparisons. These results are divided into two parts: one part regards the comparison for the whole investigated time period from 2001 till 2005. The other part presents the results for two time periods containing days with high geomagnetic and solar activity. Finally in Sec. 5 we summarize the main conclusions obtained from this work.

2. Data

2.1. IMAGE RPI Data

The NASA IMAGE (Imager for Magnetopause-to-Aurora Global Exploration) mission was launched on 25 March 2000 and successfully operated until December 2005. Its task was primarily to study the global response of the geomagnetic field to solar wind variations. IMAGE was placed in a 14.2 hours period highly eccentric polar orbit with a perigee radius of around 7500 km and an apogee radius of ca. 52200 km (8.25 ER). Further information about the IMAGE mission can be found e.g. in Reinisch et al. (2001; 2008) and Goldstein et al. (2003).

For the studies presented in this paper, a large number of electron density data, obtained from IMAGE RPI (Radio Plasma Imager) passive mode observations, are used. The amplitudes of the signals received by RPI on board of IMAGE satellite during passive mode observations can be displayed as a function of frequency and time to form a dynamic spectrum (Galkin et al., 2004). As described by Webb et al. (2007) a semi-automated fitting technique has been developed to extract electron density values and to prepare the database from these dynamic spectra. The fitting method considers physical features found in the dynamics spectra, such as the upper-hybrid band, the continuum edge, and banded emissions. Only data in the Level Zero Telemetry L0 format has been used. This limited the dates of density measurements to roughly between the beginning of 2001 to the end of 2005. Finally a database of about 205000 electron density measurements was created for this time period. Detailed information about the RPI data can be found in Webb et al. (2007), Denton et al. (2012) and at http:ulcar.uml.edu/rpi.html.

Besides electron densities and observation epochs (year, month, day, DOY, UTC time) the IMAGE/RPI data file contains locations of the observation points in Cartesian solar magnetic coordinates in Earth's radii, as well as in magnetic local time in hours and magnetic latitude in degrees. Furthermore, the IMAGE/RPI data file contains the *L*-shell distance, calculated from solar magnetic coordinates and magnetic latitude, assuming a dipole magnetic field, and the electron plasma frequency in kHz. In order to make the IMAGE/RPI data comparable to the CHAMP data (cf. Sec. 2.2) the IMAGE data in a pre-step were converted from magnetic latitude and magnetic local time into geographic latitude and longitude.

2.2. CHAMP Reconstructed Electron Density Profiles

The German minisatellite CHAMP (CHAllenging Minisatellite Payload) (cf. Reigber et al., 2000) was launched on July 15, 2000 from Plesetsk, Russia, and was used for atmospheric and ionospheric research, as well as for other geoscientific investigations. CHAMP concluded its mission and re-entered into the Earth's atmosphere on 19 September 2010.

The CHAMP orbit was almost circular and near polar with an inclination of ~87 degrees and an initial altitude of 454 km that decreased during the mission lifetime. The GPS measurements recorded on board CHAMP, with a sampling rate of 0.1 Hz, were primarily used for precise orbit determination. Besides that task, these measurements have also been exploited at German Aerospace Centre (DLR), Neustrelitz, to reconstruct the three dimensional electron density structure in the region above the CHAMP orbit up to the GPS altitude in operational mode. The CHAMP GPS data have been received at the DLR Remote Sensing Data Center Neustrelitz. Orbit information provided by GFZ Potsdam entered as the second major input into the reconstruction. During the processing of the GPS data, the calibrated link-related TEC has been calculated. In order to obtain local electron density information from the integral TEC measurements, the calibrated link-related TEC data derived for each full CHAMP revolution has been assimilated into the Parameterized Ionospheric Model (PIM) (cf. Daniell et al., 1995). For assimilation, an iterative algebraic reconstruction technique has been applied. A full revolution took ~93 minutes. Up to 4000 radio links between CHAMP and the GPS satellites were available per revolution period (cf. Fig. 1). Heise (2003) and Heise et al. (2002) describe the method in more details.

The result of the assimilation process is an improved model output presenting the 93 minutes picture of the 3D topside ionosphere and plasmasphere. The approach is working locally, meaning that areas far away from the available CHAMP-GPS links remain completely unaffected and display therefore the pure background model output. The data coverage and thus also the influence of the assimilation procedure reach their maximum inside and near the CHAMP orbit plane. For this reason, the present study uses only the reconstructed electron density profiles along the mean longitude of the CHAMP orbit plane during a full CHAMP revolution. To calculate these profiles from the 3D reconstruction, firstly the mean earth-fixed longitude of the CHAMP orbit plane, λ_{CH}, during the full revolution is determined. Thereafter a 2D electron density latitude-altitude-map is deduced from the 3D reconstruction fixing the longitude to λ_{CH}. The result is a CHAMP 2D reconstruction file containing the reconstructed electron density profiles along the mean CHAMP orbit plane longitude λ_{CH} (cf. Fig. 2).

Besides the electron density values, the CHAMP 2D reconstruction files contain the start and end times of the assimilation period (year, month, day, UTC time); duration; the mean longitude of the CHAMP orbit plane, λ_{CH}, in degrees. Additionally, the array of latitudes in degrees (for the CHAMP reconstructions, special latitudes counting from 0° at the equator at longitude equal λ_{CH}, via 90° at North Pole and 270° at South Pole to 360° back at the starting point at equator) and the array of geocentric distances in km, presenting the locations of the electron density values, are given in the CHAMP 2D reconstruction files. This latitude-altitude grid is equal for all CHAMP 2D reconstruction files and is called CHAMP 2D reconstruction grid throughout this paper.

2.3. CHAMP Orbit Files

CHAMP orbit files provided by GFZ Potsdam in CHORB format (cf. CHORB, 2001) were used here to calculate the CHAMP geocentric position vectors at IMAGE observation epochs.

3. Coincidence Criteria and Approach for Coincidence Analysis

3.1. Coincidence Criteria

For the studies presented in this paper, the following criteria were defined in order to declare an IMAGE/RPI observation to be coincident with a CHAMP 2D reconstruction file:

1. The geographic longitude of the IMAGE/RPI observation point is within a $\pm 12°$ range of the mean CHAMP orbit plane longitude:

$$\lambda_{CH} - 12^0 \leq \lambda_{IM} \leq \lambda_{CH} + 12^0 \quad (1)$$

where:

λ_{CH} is the mean geographic longitude of the CHAMP orbit plane

λ_{IM} is the geographic longitude of IMAGE observation point

2. The epoch of the IMAGE observation lies within the CHAMP reconstruction period, i.e. the Universal Time (UT) of the IMAGE epoch is between the start and the end of the CHAMP data assimilation period:

$$UT_{begin} \leq UT_{IMAGE} \leq UT_{end} \quad (2)$$

3. At one IMAGE observation epoch, the geocentric position vectors of the IMAGE observation point and the CHAMP satellite enclose not more than a certain angle, $\Delta\gamma$:

$$\omega_{IM\_CH} \leq \Delta\gamma \quad (3)$$

For example, for $\Delta\gamma = 40$ degrees, the third criterion means that the slant TEC, assimilated into PIM at grid points close to the IMAGE observation position, was measured by CHAMP within the time period of about $\pm$ 10 minutes around the IMAGE observation epoch (according to CHAMP orbital speed to move 40° during that time span). Within the studies for this paper different angle bounds are discussed (cf. Sec. 4).

Once an IMAGE/RPI observation is detected to be coincident with a CHAMP 2D reconstruction file, the position of this IMAGE/RPI observation has to be projected into the plane of the CHAMP 2D reconstruction. Thereafter the electron density value at this projection point is interpolated in the CHAMP 2D reconstructions grid. The mathematical approach for this procedure is described in the next two subsections.

3.2. Projection of the IMAGE Observation Position Vector into the Plane of the Coincident CHAMP 2D Reconstruction

As described in Sec. 2.1, the original IMAGE/RPI data were transformed from magnetic latitude and local time into geographic latitude and longitude. The geocentric radial distances of the IMAGE observation points were computed as magnitudes of the IMAGE position vectors, whose

components are given in units of Earth radii. The geocentric position vector of an IMAGE observation point can thus be computed from spherical coordinates:

$$\vec{R}_{IM} = 6378.14km \cdot R_{IM} \cdot \begin{Bmatrix} \cos\phi_{IM} \cdot \cos\lambda_{IM} \\ \cos\phi_{IM} \cdot \sin\lambda_{IM} \\ \sin\phi_{IM} \end{Bmatrix} \quad (4)$$

where:

$\vec{R}_{IM}$ … position vector of IMAGE observation point

$6378.14km$ … Earth radius according to definition in the IMAGE file

R_{IM} … geocentric radial distance of IMAGE observation point in Earth radii

ϕ_{IM} … geographic latitude of IMAGE observation point

λ_{IM} … geographic longitude of IMAGE observation point

As detailed in Sec. 2.2, the CHAMP electron densities are given on a "disk" representing the polar plane of the mean CHAMP longitude, in a circular grid in terms of geocentric radial distances and latitudes counted from the equator (i.e. 0°) via North- and South-Pole (i.e. 90° and 270° respectively) back to the equator (i.e. 360°), counter-clockwise with latitude steps of 3 degrees.

In order to compare an IMAGE electron density value with corresponding CHAMP electron densities, the IMAGE position vector has first to be projected into the plane of the coincident CHAMP 2D reconstruction "disk". The steps to achieve this are as follows:

The unit normal vector to the CHAMP reconstruction plane (cf. Fig. 3) is given by

$$\vec{\varepsilon}_{CH} = \vec{\varepsilon}_0 \times \vec{\varepsilon}_{90} = \begin{Bmatrix} \sin\lambda_{CH} \\ -\cos\lambda_{CH} \\ 0 \end{Bmatrix}, \quad (5)$$

where: $\vec{\varepsilon}_0 = \{\cos\lambda_{CH}, \sin\lambda_{CH}, 0\}$ and $\vec{\varepsilon}_{90} = \{0,0,1\}$ are the unit vectors pointing from geocentre to the equator at λ_{CH} and to the North Pole respectively. Using $\vec{\varepsilon}_{CH}$, the orthogonal projection vector $\vec{P}_{IM}$ of the IMAGE observation point position vector $\vec{R}_{IM}$ onto the CHAMP reconstruction plane (cf. Fig. 4) can be computed applying Eq. (6):

$$\vec{P}_{IM} = \vec{R}_{IM} - \left(\vec{R}_{IM} \cdot \vec{\varepsilon}_{CH}\right) \cdot \vec{\varepsilon}_{CH} \quad (6)$$

The geocentric radial distance of $\vec{P}_{IM}$ in the CHAMP reconstruction plane is simply the magnitude $\left|\vec{P}_{IM}\right|$. Since $\vec{P}_{IM}$ is lying in the CHAMP reconstruction plane, its longitude is simply λ_{CH}. For the computation of the 360° latitude on the CHAMP reconstruction plane the following formula can be employed:

$$\phi_{IM} = \arctan\left(\frac{\left(\vec{P}_{IM}\cdot\vec{\varepsilon}_{90}\right)}{\left(\vec{P}_{IM}\cdot\vec{\varepsilon}_{0}\right)}\right) = \arctan\left(\frac{P_{IM_z}}{P_{IM_x}\cdot\cos\lambda_{CH} + P_{IM_y}\cdot\sin\lambda_{CH}}\right) \qquad (7)$$

The orthogonal projected IMAGE observation point position vector $\vec{P}_{IM}$, obtained from Eq. (6), has always a shorter radial distance than the IMAGE observation point vector $\vec{R}_{IM}$. In this way, one systematically ends up with lower IMAGE radii in the CHAMP grid, at which the interpolations (cf. Sec. 3.3) between the grid points will be done. Systematically interpolating at lower radii means systematically obtaining higher CHAMP electron densities as would be appropriate for the true IMAGE altitudes. Results from comparison test runs with the orthogonal projection $\vec{P}_{IM}$ indeed indicate that the orthogonal projection is not optimal for the coincidence analysis. Thus a further step is introduced to calculate an adequate projection of the IMAGE observation position vector into the CHAMP 2D reconstruction plane: The idea is to lengthen the orthogonal projection $\vec{P}_{IM}$ in order to obtain the projection vector $\vec{\Gamma}_{IM}$ with the same *L*-shell distance as $\vec{R}_{IM}$. The *L*-shells are aligned to the geomagnetic field. Thus the deviation of the geomagnetic pole from the geographic North Pole has to be accounted for when calculating the geocentric radial distance in the CHAMP reconstruction grid corresponding to the *L*-shell of the IMAGE observation point $\vec{R}_{IM}$.

The following constant values of the geographic position of the northern geomagnetic pole (Davies, 1990) were used for the computation of the CHAMP reconstruction files (Heise et al., 2002) and had consequently also to be taken here in the coincidence analysis, in order to be consistent with the geomagnetic pole definition used for the establishment of the CHAMP reconstruction files:

$$\phi_m = 79^0.1 \quad , \quad \lambda_m = 289^0.1 \qquad (8)$$

By using the values of Eq. (8), a unit vector pointing from geocentre to the northern geomagnetic pole is given as:

$$\vec{\varepsilon}_m = \begin{Bmatrix} \cos\phi_m\cdot\cos\lambda_m \\ \cos\phi_m\cdot\sin\lambda_m \\ \sin\phi_m \end{Bmatrix} \qquad (9)$$

The geomagnetic latitudes Φ_{IM} and Φ_P of the vectors $\vec{R}_{IM}$ and $\vec{P}_{IM}$ can be computed through the dot products of these vectors with $\vec{\varepsilon}_m$:

$$\cos^2\Phi_{IM} = 1-\sin^2\Phi_{IM} = 1-\left(\frac{\vec{R}_{IM}}{\left|\vec{R}_{IM}\right|}\cdot\vec{\varepsilon}_m\right)^2 \quad , \quad \cos^2\Phi_P = 1-\sin^2\Phi_P = 1-\left(\frac{\vec{P}_{IM}}{\left|\vec{P}_{IM}\right|}\cdot\vec{\varepsilon}_m\right)^2 \tag{10}$$

Next, compute the *L*-shell value (e.g. Davies, 1990) of the IMAGE observation point by using the geomagnetic latitude Φ_{IM} derived from its position vector $\vec{R}_{IM}$, Eq. (10):

$$L_{IM} = \frac{\left|\vec{R}_{IM}\right|}{\cos^2\Phi_{IM}} \tag{11}$$

Thereafter, compute with the *L*-shell value of $\vec{R}_{IM}$, Eq. (11), and the geomagnetic latitude Φ_P of $\vec{P}_{IM}$, Eq. (10), the radial distance r_{IM}, which, along the direction of $\vec{P}_{IM}$, corresponds to the *L*-value of $\vec{R}_{IM}$:

$$r_{IM} = L_{IM}\cdot\cos^2\Phi_P \tag{12}$$

Finally, re-scale $\vec{P}_{IM}$ to the magnitude of r_{IM}:

$$\vec{\Gamma}_{IM} = \frac{r_{IM}}{\left|\vec{P}_{IM}\right|}\cdot\vec{P}_{IM} \tag{13}$$

The derived *L*-shell preserving projection vector $\vec{\Gamma}_{IM}$ has the same direction as $\vec{P}_{IM}$ and indicates in the CHAMP reconstruction grid the *L*-shell corresponding to the *L*-shell of the IMAGE observation position $\vec{R}_{IM}$. The related CHAMP latitude ϕ_{IM}, which is identical for $\vec{\Gamma}_{IM}$ and $\vec{P}_{IM}$, is computed by Eq. (7).

3.3. Interpolating an Electron Density Value in the CHAMP Reconstruction Grid at the Projected IMAGE Observation Point

With the *L*-shell preserving IMAGE observation point coordinates (r_{IM}, ϕ_{IM}) (cf. Eqs. (7) and (12)), a corresponding CHAMP electron density value can now be interpolated in the CHAMP reconstruction grid. Three interpolation methods were tried out:

1. IONEX grid interpolation scheme (Schaer et al., 1998).
2. Quadratic interpolation (Junkins et al., 1973; Komjathy, 1997).
3. Weighted Mean of Inverse Point Distance (Shepard, 1968, first formula using u=1).

Optionally, the weights of all interpolation schemes were superimposed with exponential weights according to radial distance, since the plasmaspheric electron density decays not linearly but exponentially with increasing altitude.

It turned out that the three interpolation methods, with and without superimposition by exponential weights for height, provided all very similar results. CHAMP electron density values obtained with the distinct interpolation methods differed by less than 1% of the total electron density value at identical interpolation points. – Thus for all results presented in the following sections, the IONEX grid interpolation, with exponential weights for the heights, was used.

3.4. Statistical Approach for the IMAGE vs. CHAMP Comparison

For each detected coincidence between an IMAGE/RPI observation and a CHAMP 2D reconstruction file, the position of the IMAGE/RPI observation was projected into the plane of the CHAMP 2D reconstruction. Thereafter the electron density value at this projection point was interpolated in the CHAMP reconstructions grid applying the IONEX grid interpolation scheme. In the last step the difference between the electron density interpolated in the CHAMP 2D reconstruction grid at the IMAGE projection point, $Ne(CH)$, and the IMAGE/RPI observed electron density, $Ne(IM)$, was calculated. This procedure resulted in a series of electron density differences (EDD):

$$dNe = Ne(CH) - Ne(IM) \tag{14}$$

In addition to the EDD, Eq. (14), relative EDD w.r.t. the mean of CHAMP and IMAGE electron density were investigated:

$$dNe_{\%} = \frac{Ne(CH) - Ne(IM)}{\frac{Ne(CH) + Ne(IM)}{2}} * 100\% = \frac{2 \cdot dNe}{Ne(CH) + Ne(IM)} * 100\% \tag{15}$$

For statistical analysis of the CHAMP minus IMAGE EDD, in a pre-step the Mean and the Standard Deviation (STD) of the differences were computed, and the difference values outside of the $Mean \pm 2.576 \cdot STD$ bounds margin were excluded from the analysis. Assuming a Gaussian distribution of the difference values, these margins lead to exclusion of about 1% of all values. This was performed in order to avoid a distortion of the statistical values through extreme outliers.

In the following, the Median values in combination with the RMS of the EDD, relative EDD and absolute values $|dNe|$ and $|dNe_{\%}|$ were evaluated and analysed. In addition, the 90% bounds of the absolute values $|dNe|$ and $|dNe_{\%}|$ were computed, by sorting of the absolute values and calculating the nine tenths bound.

4. Results

As pointed out in Sec. 3.1, the third coincidence criterion allows a variable angle bound, $\Delta\gamma$, for the angle, ω_{IM_CH}, enclosed by the geocentric position vectors of the IMAGE and CHAMP satellites at the considered epoch. Within the studies for this paper, different values for $\Delta\gamma$ were tried. Thereby no notable distinctions between the statistical results for different values of $\Delta\gamma$ were observed. Therefore, the majority of the results presented in this paper refer to the angle bound $\Delta\gamma = 180°$, meaning that there were effectively no restrictions on the angle ω_{IM_CH}.

However, additional selected results for the angle bound of $\Delta\gamma = 40°$ will be presented too. These outcomes are always extra marked in the paper. All other results, where the angle bound is not explicitly given in the text, refer to the unbounded angle ω_{IM_CH}.

For further investigations, the same version of the PIM model (Daniell et al., 1995), as had been employed for the CHAMP reconstructions (cf. Sec. 2.2), was also used here to calculate model electron density values at the CHAMP 2D reconstruction grid points. The result were PIM electron density profiles in the same 2D grid as for the investigated CHAMP 2D reconstructions. Using the same coincidence criteria as for the CHAMP-IMAGE comparison (cf. Sec. 3.1) and again the *L*-shell preserving projection to map the IMAGE observation points into the PIM 2D plane (cf. Sec. 3.2), the absolute and relative differences between the electron density interpolated in the 2D PIM grid at the IMAGE projection point, $Ne(PIM)$, and the IMAGE/RPI observed electron density, $Ne(IM)$, were calculated according to:

$$dNe^{PIM} = Ne(PIM) - Ne(IM) \tag{16}$$

$$dNe^{PIM}_{\%} = \frac{Ne(PIM) - Ne(IM)}{\frac{Ne(PIM)+Ne(IM)}{2}} * 100\% = \frac{2 \cdot dNe^{PIM}}{Ne(PIM) + Ne(IM)} * 100\% \tag{17}$$

4.1. Whole Investigated Time Period 2001-2005

In this subsection the comparison outcomes for the whole investigated time period are presented. In the first part of the subsection the overall results for all altitudes up to GPS orbit height are given. Then, in addition, the CHAMP/PIM and IMAGE EDD are compared in the region $1<L<3$, which is the most dominant part particularly with regard to the TEC calculation, as well as separately in the regions $3<L<4$, and $4<L<8$. Finally selected comparison results for a restricted angle ω_{IM_CH} are shown.

Assuming no restrictions on the angle ω_{IM_CH}, the overall number of coincidences within the whole investigated time period is around 7380. Fig. 5 presents the distribution of the absolute values of the CHAMP-IMAGE EDD $|dNe|$ on the left hand side and of the absolute values of the PIM-IMAGE EDD $|dNe^{PIM}|$ on the right hand side. Additionally, the Median, RMS and the 90% bound values of the absolute values are displayed, all in cm^{-3}. Here the presentation of the absolute values was chosen to simplify the comparison of the Median values between PIM and CHAMP, because the EDD are not normal distributed (cf. Fig. 6). An improvement w.r.t. all given statistical values can be observed comparing pure model with the reconstructions results.

Fig. 6 depicts the distribution of the CHAMP-IMAGE EDD (cf. Eq. (14)), the Median, RMS, and the 90% bound (90% bound is related to $|dNe|$) values. Conspicuous is the slower decrease of sample numbers on the negative side from the Mean, indicating that a not negligible part of the electron densities interpolated from the CHAMP 2D reconstructions are partly lower than the corresponding IMAGE electron density values.

In order to get a better impression about the magnitude of the compared electron density (ED) values in the $L_{IM} > 3$ region, Fig. 7 shows the scatterplots of the IMAGE versus CHAMP ED for

L-shell distances (from top to bottom): $1 < L_{IM} < 3$, $3 < L_{IM} < 4$ and $4 < L_{IM} < 8$. Whereas for the region $1 < L_{IM} < 3$, the ED values range mainly between 1000 and 6000 cm^{-3}, the ED rapidly decrease in the *L*-shell region above 3 ER. The ED range between 0 and 1200 cm^{-3} for $3 < L_{IM} < 4$ and between 0 and 300 cm^{-3} for $4 < L_{IM}$. At the same time, an increasing asymmetry appears between the CHAMP ED and the IMAGE ED w.r.t. the scatter plot diagonal (blue line in Fig. 7) with increasing *L*-shell distance, indicating systematically lower CHAMP ED compared to the IMAGE ED with increasing altitude.

The next three figures visualize the comparison results for the different *L*-shell distance regions, investigating the relation between the distribution of the relative EDD (cf. Eqs. (15) and (17)) and the corresponding position of the projected IMAGE observation point in terms of geographic latitude ϕ_{IM} (cf. Eq. (7)) and *L*-shell distance L_{IM} (cf. Eq. (11)). Fig. 8 considers the most interesting area, depicting the relative EDD for the *L*-shell distances between 1 and 3 ER. The left column subfigures in blue show the relative CHAMP-IMAGE EDD $dNe_{\%}$ values (top) and the relative PIM-IMAGE EDD $dNe_{\%}^{PIM}$values (bottom) versus ϕ_{IM}. The right column subfigures in red depict the distribution of the relative CHAMP-IMAGE EDD (top) and the relative PIM-IMAGE EDD (bottom) as well as Median and RMS of the EDD for this *L*-shell distance interval. We observe nearly normal distributed relative differences (for both reconstruction and background model) with a Median value around -3% for CHAMP and around 8% for PIM. The comparison of the right hand side subfigures reveals indeed a decrease of all statistical values, achieved by the CHAMP assimilation procedure. The latitudes of the positions of the coincidence points range between around $\pm 50°$. Further, a slight tendency of the relative differences towards the negative values with latitudes moving away from the equator, is observable. The total number of coincidences is here around 3070, i.e. slightly less than half of the overall number of coincidences.

Similar to the left column of the previous figure, Fig. 9 investigates the CHAMP $dNe_{\%}$ values in dependency of ϕ_{IM} and L_{IM} for the *L*-shell distance regions above 3 ER. The left column subfigures in blue show the $dNe_{\%}$ values versus ϕ_{IM} for the *L*-shell distances (from top to bottom): $3 < L_{IM} < 4$ and $4 < L_{IM} < 8$. The right column subfigures in red depict distribution of the $dNe_{\%}$ values as well as Median, RMS and 90% bound of the relative EDD for the same *L*-shell distance intervals. Fig. 10 depicts distribution of the $dNe_{\%}^{PIM}$ values as well as Median, RMS and 90% bound of the relative PIM-IMAGE EDD, again for the same *L*-shell distance intervals.

Fig. 10 clearly shows that the PIM electron densities in the *L*-shell interval from 4 to 8 ER are much lower than the corresponding IMAGE electron density values. The PIM model seems to underestimate the electron density values at these high altitudes around the plasmapause. As expected, the CHAMP measurements coverage and the measurements accuracy seem to be insufficient to compensate this background caused underestimation within the assimilation process. Comparing the two corresponding subfigures of Fig. 9 and Fig. 10, no significant differences are notable with regard to the statistics for the relative EDD. Obvious is the shift of the relative differences from 0% to -190% with growing *L*-shell distances for both PIM and CHAMP. The $dNe_{\%}$ values appear mainly in the latitude ranges between -60° and -20° North and from 20° to 50° North. On *L*-shell scale, the relative EDD between -150% and -200% are primarily visible in the interval $4 < L_{IM} < 8$.

Concluding the results displayed in Figs. 7 – 10, a good correlation between IMAGE/RPI data and CHAMP reconstructions can be observed for the *L*-shell distances below 3 ER. In this region the CHAMP assimilation procedure leads to an obvious decrease of the EDD compared to the EDD using the pure PIM model. In the *L*-shell region above 4 ER the quality of a background model is of crucial importance, since the rather poor CHAMP measurements coverage, limited measurements accuracy (compared to the ED value magnitudes in this region) and non-optimal observation geometry make it difficult to compensate the shortcomings of a background. Proper data assimilation, especially for the region above 4 ER, would require measurement rays from many different directions (i.e. better observation geometry which was at plasmapause altitudes not given with the available CHAMP-GPS constellation), and ideally additional measurements.

Fig. 11 illustrates the vertical behavior of CHAMP reconstructed (in red) and PIM modeled (in blue dashed) electron densities at 39° N geographic latitude. Additionally, the corresponding IMAGE/RPI electron densities are presented in green color; here the locations of the observations correlate of course not exactly with the profiles latitude/longitude. The IMAGE longitude/latitude is in the range of $\pm 10°/\pm 3°$ of the CHAMP and PIM profile longitude/latitude; the *L*-shell distances of the IMAGE/RPI observations are between 5 and 6.5 ER. Here again the underestimation of the background model is visible. The CHAMP reconstructed profile seems to map the plasmapause much better than the model.

For further elaboration of the results of this section, we compared the CHAMP reconstructions and the IMAGE measurements also for the angle ω_{IM_CH} bounded by 40° (cf. Sec. 3.1, third coincidence criterion). Comparing the distribution of the (relative) CHAMP-IMAGE EDD as well as Median, RMS and 90% bound values for the unbounded angle ω_{IM_CH}, and those for the angle ω_{IM_CH} bounded by 40°, no significant differences could be observed. The same holds for the comparison of the relation between the distribution of the $dNe_{\%}$ values and geographic latitude ϕ_{IM} or *L*-shell distance L_{IM} for bounded and unbounded angles ω_{IM_CH}.

4.2. Results for Storm Days

Beside the investigations on statistics of the comparison between CHAMP and IMAGE/RPI data for the whole time period of 5 years, containing days with different ionospheric conditions, two time periods including days of high geomagnetic and moderate to high solar activity were analysed separately. The results presented in this subsection again pertain to no restrictions on the angle ω_{IM_CH}.

The two investigated time periods are:

1. 14.06.2001 - 26.06.2001, including days with a solar flux number, F10.7, over 220 flux units and a global planetary geomagnetic 3^h index Kp over 5.

2. 07.05.2005 – 17.05.2005, including days with F10.7 over 120 and Kp values over 8.

Fig. 12 depicts the distribution of the absolute values of the EDD for these two time periods. The left hand side column shows the values for the first time period: the absolute values of CHAMP-IMAGE EDD $|dNe|$ on the top subfigure and the absolute values of PIM-IMAGE EDD

$|dNe^{PIM}|$ on the bottom subfigure. The right hand side column shows the values for the second time period in the same order. Additionally, the Median, RMS and the 90% bound values of the absolute values of the EDD are displayed, all in cm^{-3}. The overall number of coincidences within the first time period is around 730, and around 320 for the second time interval.

Comparing the CHAMP statistics for the whole time period (cf. Fig. 5, left) with the corresponding CHAMP results for the two investigated time intervals here (cf. Fig. 12, top row), a decrease of all statistical values can be observed for the first time span. Based on investigations of the relation between the distribution of the EDD values and the *L*-shell distances L_{IM} (cf. Eq. (11)) of the corresponding projected IMAGE observation points, the authors attribute this decrease to the comparatively small number of projected IMAGE observation points in the *L*-shell distances region above 4 ER. For the second time interval the Median values remain almost unchanged, whereas the RMS and the 90% bound values increase, probably due to disturbances.

Comparing the CHAMP statistics (cf. Fig. 12, top row) with the corresponding PIM results (cf. Fig. 12, bottom row) a clear improvement w.r.t. all given statistical values can be observed except for the 90% bound for the first time period. The improvements are in particular visible within the second time interval: Whereas for the whole time period the improvements of the Median, RMS and the 90% bound values, comparing pure PIM model with the reconstructions results, range between around 9 (Median), 41 (RMS) and 69 (90% bound) cm^{-3} (cf. Fig. 5); for the second time period the improvements range between around 87 (Median), 71 (RMS) and 95 (90% bound) cm^{-3}. Fig. 13 visualizes these improvements, showing the Median, RMS and 90% bound values of the absolute values of EDD for the whole investigated time period on the left hand side and for the second disturbed time period (07. – 17.05.2005) on the right hand side. PIM values are presented in dark blue, CHAMP values in pale blue.

5. Conclusions

Using IMAGE/RPI passive mode electron density data, we have systematically validated the reconstructed CHAMP electron density profiles that are derived by assimilation of CHAMP-GPS observations into the PIM model.

Comparing the absolute values of the electron density differences (EDD) between CHAMP and IMAGE with the EDD between PIM and IMAGE for the whole investigated time period (2001-2005), a ~5% decrease of the Median, RMS, and 90% bound values is observed induced by the CHAMP assimilation procedure (cf. Fig. 5). For two selected time periods with high geomagnetic and solar activity, a decrease of up to 30% was notable (cf. Figs. 12, right column). This demonstrates the potential of data assimilation compared to the pure background model, especially under disturbed conditions.

The results presented in this paper clearly demonstrate the strengths of TEC data assimilation from LEO spacecraft. On the other hand, they also reveal deficiencies of this technique regarding the background model used and the limited capability of observation data assimilation to compensate for this in regions sparsely covered by observables and/or with degraded observation geometry.

A good correlation between IMAGE/RPI data and CHAMP reconstructions is observed for the *L*-shell distances below 3 Earth's radii, which is the most dominant part particularly with regard to

the TEC calculation. For this region, the Median of the relative CHAMP-IMAGE EDD is about -3%, while the Median of the relative PIM-IMAGE EDD is around 8%. Hence CHAMP reconstructions provide a good database for the modelling of the topside ionosphere and plasmasphere.

At high altitudes around the plasmapause the PIM model seems to underestimate the electron density values. It is important to note that, for all results presented in this contribution, the same old version of the PIM model (Daniell et al., 1995) was used, that had been employed for the CHAMP reconstructions. In the $L>4$ region the rather poor CHAMP measurements coverage, the limited accuracy of the assimilated observations and the non-optimal CHAMP measurements geometry clearly seem not to be strong enough to compensate this underestimation within the assimilation process. For modelling of this upper part of the plasmasphere, the use of additional measurements, e.g. the plasmagrams obtained from IMAGE RPI active mode observations (Reinisch et al., 2009), is recommended.

One important result of our work was making very different data sources comparable. Coincidence criteria and an approach for coincidence analysis were developed, including different suggestions and discussions for projection and interpolation methods of the IMAGE data into the geographic domain of the CHAMP reconstructions. The detailed description of this part of the work included in the present contribution may be helpful for comparable studies of similar data sets.

Acknowledgments:

Work at Dartmouth College (R.E. Denton) was further supported by the US National Science Foundation grant ATS 1105790.
The authors are very grateful to all colleagues of the CHAMP team.

References

(Belehaki et al., 2003) Belehaki, A., Jakowski, N., Reinisch, B. Comparison of Ionospheric ionization measurements over Athens using ground ionosonde and GPS derived TEC values. Radio Science, 38, 6 (DOI 10. 1 029/2003RS002868), 2003.

(CHORB, 2001) Format Description: The CHAMP Orbit Format CHORB, DOC: CH-GFZ-FD-002 (2001), available via http://www-app2.gfz-potsdam.de/pb1/op/champ/docs_CHAMP/CH-GFZ-FD-002.pdf

(Daniell et al., 1995) Daniell, R.E, Brown, L.D., Anderson, D.N., Fox, M.W., Doherty, P.H., Decker, D.T., Sojka, J.J., Schunk, R.W. Parameterized ionospheric model: a global ionospheric parameterization based on first principles models. Radio Sci., 30, 1499-1510, 1995.

(Davies, 1990) Davies, K. Ionospheric Radio. Vol. 31 of IEE Electromagnetic Wave Series, Peter Peregrinus Ltd., ISBN 0 86341 186 X, 1990.

(Denton et al., 2012) Denton, R. E., Wang, Y., Webb, P. A., Tengdin, P. M., Goldstein, J., Redfern, J. A., Reinisch, B.W. Magnetospheric electron density long-term (>1 day) refilling rates

inferred from passive radio emissions measured by IMAGE RPI during geomagnetically quiet times. J. Geophys. Res., 117, A03221, doi:10.1029/2011JA017274, 2012.

(Galkin et al., 2004) Galkin, I., Reinisch, B. W., Grinstein G., Khmyrov, G., Kozlov, A., Huang, X., and Fung, S. F. Automated exploration of the radio plasma imager data. J. Geophys. Res., 109(A12), A12210, doi:10.1029/2004JA010439, 2004.

(Goldstein et al., 2003), Goldstein, J., Spasojević, M., Reiff, P. H., Sandel, B. R., Forrester, W. T., Gallagher, D. L., Reinisch, B. W. Identifying the plasmapause in IMAGE EUV data using IMAGE RPI in situ steep density gradients. Journal Of Geophysical Research, Vol. 108, No. A4, 1147, doi: 10.1029/2002JA009475, 2003.

(Heise et al., 2002) Heise, S., Jakowski, N., Wehrenpfennig, A., Reigber, Ch., Lühr, H. Sounding of the topside ionosphere/plasmasphere based on GPS measurements from CHAMP: Initial results. Geophysical Research Letters, 29(14), DOI: 10.1029/2002GL014738, 2002.

(Heise, 2003) Heise, S. Rekonstruktion dreidimensionaler Elektronendichteverteilungen basierend auf CHAMP-GPS-Messungen (in German). PhD Thesis, Freie Universität Berlin, Germany, online available via http://www.diss.fu-berlin.de/diss/receive/FUDISS_thesis_000000000584, 2003.

(Jakowski et al., 1991) Jakowski N., Jungstand, A., Lois, L., Lazo, B. Night-time enhancements of the F2-layer ionization over Havana. J. Atmos. Terr. Phys., 53, 1131-1138, 1991.

(Jakowski et al. 2007) Jakowski, N., Wilken V., Mayer C. Space weather monitoring by GPS measurements on board CHAMP. Space Weather, 5, S08006, doi:10.1029/2006SW000271, 2007.

(Junkins et al., 1973) Junkins, J.L., Miller, G.W., Jancaitis, J.R. A Weighting Function Approach to Modeling of Irregular Surfaces. Journal of Geophysical Research, Vol. 78. No. 11, 1973.

(Komjathy, 1997) Komjathy, A. Global Ionospheric Total Electron Content Mapping Using the Global Positioning System. Ph.D. dissertation, Department of Geodesy and Geomatics Engineering Technical Report No. 188, University of New Brunswick, Fredericton, New Brunswick, Canada, 1997.

(Lunt et al., 1999) Lunt, N., L. Kersley, G. J. Bishop, A. J. Mazzella, and G. J. Bailey. The effect of the protonosphere on the estimation of GPS total electron content: Validation using model simulations. Radio Sci., 34(5), 1261-1271, 1999.

(Poletti-Liuzzi et al., 1976) Poletti-Liuzzi, D. A., Yeh, K. C., Liu, C. H. Simulation and measurement of the plasmaspheric electron content. In: The geophysical use of satellite beacon observations, Proceedings of the Symposium, Boston, Mass., June 1-4, 1976. (A77-30501 13-46) Boston, Boston University, p. 197-218, 1976.

(Reigber et al., 2000) Reigber, Ch., Lühr, H., Schwintzer, P. CHAMP mission status and perspectives. Suppl. to EOS, Transactions, American Geophysical Union, 81(48), F307, 2000.

(Reinisch et al., 2001) Reinisch, B.W., Huang, X., Haines, D.M., Galkin, I.A., Green, J.L., Benson, R.F., Fung, S.F., Taylor, W.W.L., Reiff, P.H., Gallagher, D.L., Bougeret, J.L., Manning, R., Carpenter D.L., Boardsen S.A. First results for the Radio Plasma Imager on IMAGE. Geophysical Research Letters, Vol. 28, No. 6, 1167 – 1170, 2001.

(Reinisch et al., 2004) Reinisch, B. W., Huang, X., Song, P., Green, J. L., Fung, S. F., Vasyliunas, V. M., Gallagher, D. L., Sandel, B. R. Plasmaspheric mass loss and refilling as a result of a magnetic storm. J. Geophys. Res., 109(A1), A01202, doi:10.1029/2003JA009948, 2004.

(Reinisch et al., 2009) Reinisch, B. W., Mark, W., Moldwin, B., Denton, R. E., Gallagher, D. L., Matsui, H., Pierrard, V., Tu, J. Augmented Empirical Models of Plasmaspheric Density and Electric Field using IMAGE and CLUSTER Data. Space Sci. Rev., 145, 231-261, doi:10.1007/s11214-008-9481-6, 2009.

(Schaer et al., 1998) Schaer, S., Gurtner, W., Feltens, J. IONEX: The IONosphere Map EXchange Format Version 1. Proceedings of the IGS Analysis Centers Workshop, Darmstadt, Germany, February 9 – 11, 1998.

(Shepard, 1968) Shepard, D. A two-dimensional interpolation function for irregularly-spaced data. Proceedings of the 1968 ACM Nat. Conf., 517–524, doi:10.1145/800186.810616, 1968.

(Titheridge, 1976) Titheridge, J.E., Ion transition heights from topside electron density profiles. Planet. Space Sci., 24, 229-245, 1976.

(Webb et al., 2007) Webb, P., Benson, R., Denton, R., Goldstein, J., Garcia, L., Reinisch, B.W. An inner magnetospheric electron density database determined from IMAGE/RPI passive dynamic spectra. Eos Trans. AGU, 88(52), Fall Meet. Suppl., Abstract SM12A-04, 2007.

Figure Captions

Fig. 1: The topside radio link distribution, projected into the plane of the mean CHAMP longitude, to the visible GPS satellites during one CHAMP revolution; 09.08.2001, 3331 TEC measurements (from Heise, 2003).

Fig. 2: Example of a CHAMP reconstruction showing an one CHAMP orbit revolution picture of the ionospheric and plasmaspheric electron density in the plane of the mean CHAMP orbit longitude.

Fig. 3: The unit vectors defining the plane of mean CHAMP longitude (indicated as blue “disk”) coordinate system.

Fig. 4: The orthogonal projection $\vec{P}_{IM}$ of the IMAGE observation point position vector $\vec{R}_{IM}$ onto the CHAMP 2D reconstruction plane (displayed here edge-on as dash-dotted line).

Fig. 5: Distribution of the absolute values of the CHAMP-IMAGE (left), PIM-IMAGE (right) EDD. Additionally the Median, RMS and 90% bound values of the absolute values of the EDD are given in the upper right corners. All values in cm^{-3}.

Fig. 6: Distribution of the CHAMP-IMAGE EDD. Additionally the Median, RMS and 90% bound values are given in the upper right corner. All values in cm^{-3}.

Fig. 7: Scatterplots of IMAGE versus CHAMP ED for *L*-shell distances (from top to bottom): between 1 ER and 3 ER, between 3 ER and 4 ER, between 4 ER and 8 ER.

Fig. 8: Left hand side: Relative CHAMP-IMAGE EDD (top) and PIM-IMAGE EDD (bottom) versus geographic latitude. Right hand side: Distribution of the relative CHAMP-IMAGE EDD (top) and PIM-IMAGE EDD (bottom) for *L*-shell distances between 1 ER and 3 ER.

Fig. 9: Relative CHAMP-IMAGE EDD versus geographic latitude (left) and distribution of the relative CHAMP-IMAGE EDD (right) for *L*-shell distances (from top to bottom): between 3 ER and 4 ER, between 4 ER and 8 ER.

Fig. 10: Distribution of the relative PIM-IMAGE EDD for *L*-shell distances: between 3 ER and 4 ER (left), between 4 ER and 8 ER (right).

Fig. 11: Electron density profiles for DOY 140 of 2001 at geographic latitude of 39 °N and longitude of -6.62 °E. Reconstructed CHAMP profile in red, PIM calculated profile in blue dashed, IMAGE in green, here the observations are marked by dots.

Fig. 12: Distribution of the absolute-values of the CHAMP-IMAGE (top), PIM-IMAGE (bottom) EDD. Left column: During the first time period (14.06.2001-26.06.2001). Right column: During the second time period (07.05.2005-17.05.2005). Additionally the Median, RMS and 90% bound values of the absolute-values of the EDD are given in the upper right corners. All values in cm^{-3}.

Fig. 13: Median, RMS and 90% bound values of the absolute values of the EDD. PIM values are presented in dark-blue, CHAMP values in pale blue. Left hand side: whole investigated time period (2001-2005). Right hand side: second disturbed time period (07.05.2005-17.05.2005).